minerals

MDPI

Article

Selective Adsorption of Sodium Silicate on the Surface of Bastnaesite and Fluorite in Salicylhydroxamic Acid System under Alkaline Conditions

Maoyuan Wang [1], Wenliang Xiong [1,2,3,*], Junhui Xiao [4], Yao Guo [1,2,3], Jie Deng [1,2,3], Da Chen [1,2,3], Anni Ouyang [1], Menglin Lei [1,2,3] and Lijun Zhang [1,2,3,*]

[1] Institute of Multipurpose Utilization of Mineral Resources, Chinese Academy of Geological Sciences, Chengdu 610041, China
[2] Sichuan Rare Earth Technology Innovation Center, Chengdu 610041, China
[3] Engineering and Technology Innovation Center for Comprehensive Utilization of Strategic Minerals, Ministry of Natural Resources, Chengdu 610041, China
[4] School of Environment and Resource, Southwest University of Science and Technology, Mianyang 621010, China
* Correspondence: seanwlzm@163.com (W.X.); mangran0627@163.com (L.Z.)

Abstract: During the flotation separation process of bastnaesite, it is difficult to separate bastnaesite from fluorite effectively. In this present study, sodium silicate (SS) can effectively improve the flotation separation effect of bastnaesite and fluorite in salicylhydroxamic acid (SHA) systemasa. Through relevant analyses, such as Zeta potential measurements, adsorption capacity tests, Fourier transform infrared (FTIR) spectroscopic analyses and X-ray photoelectron spectroscopy (XPS) tests, the selective suppressor of SS on fluorite was proven. At pH 10, the single mineral flotation results show that with the increase of SS dosage, the flotation recovery of fluorite rapidly decreases from 61.5% to 35.31%, while the flotation rate of bastnaesite is still high (recovery is 80.02%). Then, the experiment of artificial mixed ore proved that the flotation separation of fluorite and bastnaesite was effective under the appropriate dosage of inhibitor. The results of potentiodynamic measurement and an adsorption capacity test showed that the $SiO(OH)_3^-$ structure of SS more easily reacted with fluorite, which further prevented the adsorption of SHA on the fluorite surface. FTIR test results and XPS analysis further showed that SS had a strong binding effect with the Ca site on the fluorite surface, but a weak binding effect with the Ce site on the bastnaesite surface. Consequently, SS can be used as an effective inhibitor in the flotation separation of fluorite and bastnaesite.

Keywords: bastnaesite; fluorite; flotation; sodium silicate; salicylhydroxamic acid

check for updates

Citation: Wang, M.; Xiong, W.; Xiao, J.; Guo, Y.; Deng, J.; Chen, D.; Ouyang, A.; Lei, M.; Zhang, L. Selective Adsorption of Sodium Silicate on the Surface of Bastnaesite and Fluorite in Salicylhydroxamic Acid System under Alkaline Conditions. *Minerals* **2023**, *13*, 69. https://doi.org/10.3390/min13010069

Academic Editor: Chiharu Tokoro

Received: 23 November 2022
Revised: 20 December 2022
Accepted: 27 December 2022
Published: 31 December 2022

Copyright: © 2022 by the authors. Licensee MDPI, Basel, Switzerland. This article is an open access article distributed under the terms and conditions of the Creative Commons Attribution (CC BY) license (https://creativecommons.org/licenses/by/4.0/).

1. Introduction

The 17 metals in the periodic table (lanthanides, scandium and yttrium) make up the rare-earth elements, which include light, medium and heavy REEs [1–3]. Due to their unique physical and chemical properties, light REEs are widely used in catalysis, superconductivity, the chemical industry and other fields. Light REEs are widely used in many fields due to their special characteristics [4]. Today, demand for light REEs is surging in many countries around the world [5,6]. China has a large amount of rare-earth resources, with about 65.88 million tons of rare-earth reserves, and the country supplies more than 90% of the world's rare-earth resources [7,8]. Normally, bastnaesite is associated with calcite, barite, fluorite, etc. How to effectively enrich bastnaesite from gangue minerals is of great importance for the development of low-grade fine bastnaesite [9,10]. Flotation separation is a highly effective method to recover slight bastnaesite, as compared to magnetic and gravity separation. Bastnaesite and fluorite have similar properties. The effective separation of fine bastnaesite from fluorite has always been a difficult problem in the field of mineral processing [11–14]. Salicylhydroxamic acid (SHA) is highly selective to bastnaesite and

is usually used as a collector in the bastnaesite flotation process. However, SHA is also selective for fluorite [15–17]. Therefore, the search for safe, effective and cost-efficient inhibitors can increase the separation efficiency of bastnaesite and fluorite. The inhibitors can provide preferential adsorption on gangue minerals due to their increased hydrophilicity and effectively prevent adsorption between collectors and mineral surface sites [18–20].

Sodium silicate (SS) is the generally used fluorite inhibitor in bastnaesite flotation, and SS has a good dispersion effect on pulp [21]. The adsorption mechanism of SS on mineral surfaces involves physical adsorption and chemical adsorption. With SS, hydrophilic and electronic silica colloidal particles and hydrogen silicate are the main inhibitors [22]. The study found that, in the flotation separation process, the absolute value of the adsorption energy of fluorite for $SiO(OH)_3^-$ was obviously higher than that of $Si(OH)_4$, and the adsorption of $SiO(OH)_3^-$ was more secure on fluorite surfaces than that of $Si(OH)_4$ [23]. It is possible that $SiO(OH)_3^-$ reacted with Ca^{2+} to form a complex, changing its hydrophilicity and, thereby, reducing the adverse effects of fluorite on the flotation of bastnaesite. Under different pH systems, SS displayed inhibitory effects with different intensities on fluorite. The difference in surface hydrophobicity was used to separate fluorite from bastnaesite [14,17].

This study used SS as an inhibitor for flotation separation of bastnaesite and fluorite, while SHA was used as a collector. The inhibition effect of SS on fluorite at a specific pH value was compared by micro-flotation experiments. At the same time, the selective inhibition effect of SS on fluorite was explained by potentiodynamic measurements, adsorption tests, infrared spectroscopy, XPS analysis and solution chemistry. Thus, the conclusion of this study can provide a theoretical basis for the development and implementation of the separation process of fine-grained bastnaesite and co-associated fluorite resources.

2. Materials and Method

2.1. Materials

The pure minerals of bastnaesite and fluorite used in the experiment were sourced from China. The single mineral utilized in the test was obtained by crushing, picking and repeatedly purifying the raw ore. The purity of the bastnaesite and fluorite was determined by chemical analysis (Tables 1 and 2) and X-ray diffraction (Figure 1), which proved that the high purity met the test requirements [24]. The test regulators (NaOH and H_2SO_4), collector (Salicylhydroxamic acid) and inhibitor (Sodium silicate) were all analytical pure.

Table 1. Chemical composition of bastnaesite powder samples (%).

Element	CeO_2	La_2O_3	Nd_2O_3	Pr_2O_3	Gd_2O_3	Sm_2O_3	Fe_2O_3
Content	34.882	29.476	7.096	2.624	0.564	0.301	1.348
Element	MoO_3	BaO	PbO	CaO	SiO_2	ThO_2	Others
Content	1.255	1.211	1.114	0.632	0.416	0.320	0.990

Table 2. Chemical composition of fluorite powder samples (%).

Element	CaO	F	SiO_2	Al_2O_3	SO_3
Content	73.177	23.705	0.172	0.022	0.020
Element	Fe_2O_3	ZnO	SrO	Y_2O_3	Others
Content	0.050	0.020	0.009	0.007	0.011

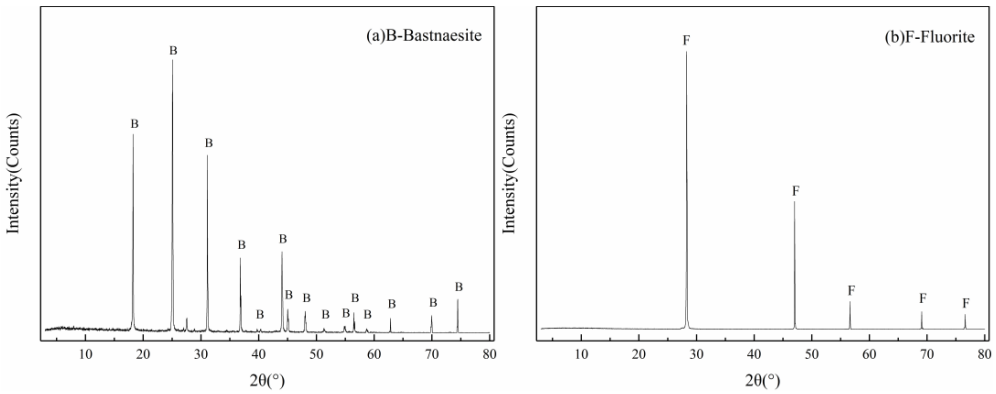

Figure 1. XRD spectra of bastnaesite (**a**) and fluorite (**b**) particles.

2.2. Micro-Flotation Tests

The pure mineral flotation tests used the XFGII hanging trough flotation machine shown in Figure 2. Each 2.00 g sample was placed in a 50 mL flotation tank before adding 35 mL deionized water and stirring for 1 min. The pH was adjusted with H_2SO_4 or NaOH for 3 min. Samples were stirred for 3 min after addition of SS and then for another 3 min with SHA. After adding the foaming agent, stir for 2 min and then flotation for 4 min. The foam products were dried and weighed [25], and the calculation formula of flotation recovery is as follows. The micro-flotation tests flow is shown in Figure 3.

$$\varepsilon = \frac{m_1}{m_1 + m_2} \times 100\% \quad (1)$$



Figure 2. XFG flotation machine used for the flotation tests.

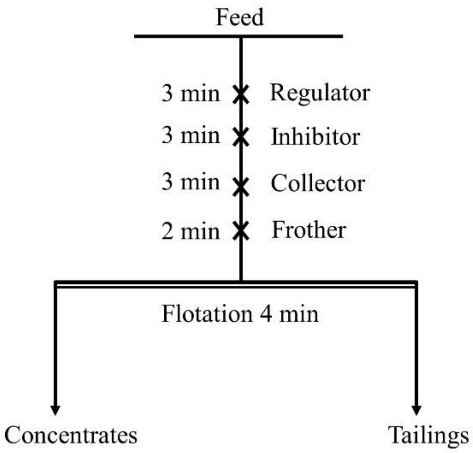

Figure 3. Flotation flow chart for minerals.

2.3. Potentiodynamic Potential Measurement

The Malvern Zeta sizer nano ZS analyzer was used to test mineral Zeta potential. The specific test steps are as follows: take 2.00 mg single mineral (−5 μm) into the conical flask, add 30 mL deionized water into it, and adjust the pulp according to the flotation process for a single mineral. It was oscillated on the thermostatic vibrating screen for 30 min and left for 10 min. The supernatant was taken to measure zeta potential. Three measurements were taken under different dose conditions, and the average of the final results was taken.

2.4. Adsorption Tests

A UV-3000 ultraviolet spectrophotometer was used to measure the adsorption capacity of the reagent on the mineral surface. A 2.00 g sample of a single mineral was weighed and placed in a conical flask for each test, and 35 mL deionized water was added. The reagent was added according to the single mineral flotation process. After shaking in a constant temperature shaker for 2 h, the supernatant was taken to determine the absorbance after solid–liquid separation, and then the concentration of the remaining reagent in the solution was calculated by the standard curve.

2.5. FTIR Measurements

Put 2.00 g single mineral sample (5 μm) into a beaker, pour 30 mL deionized water into it, add flotation agent and stir for 1 h. The mineral samples were then washed three times with deionized water. The last step is to dry in a vacuum oven (40 °C). The sample was prepared by the potassium bromide (KBr) disk method, and FTIR spectra were obtained by the IRffinity-1 Fourier Transform Infrared Spectrometer (Shimadzu, Kyoto, Japan). The region of spectral data is 400–4000 cm^{-1} [26].

2.6. XPS Analysis

Samples for XPS testing were prepared in the same manner as FTIR. XPS spectra were obtained by measuring the sample with the Thermo ScientificESCALab 250Xi XPS tester. The XPS spectra of mineral samples, before and after being treated by flotation reagent, were analyzed, and the specific adsorption sites between reagent molecules and minerals were determined.

3. Results

3.1. Micro-Flotation Results

3.1.1. Single Mineral Flotation Tests

Figure 4a shows the relationship between the collector SHA dose and mineral floatability at pH 8. The results show that when the dose of collector SHA is 4×10^{-4} mol/L, bastnaesite and fluorite reach their maximum values [10]. The results in Figure 4b show that bastnaesite and fluorite have high floatability under weak alkaline conditions with/without SS. When the pH is 8~10, the floatability of bastnaesite is better, and the floatability of fluorite is better at pH 7~8. At pH 10, the presence of SS has no obvious effect on the flotation recovery of bastnaesite, but the flotation recovery of fluorite decreases greatly. This result shows that SS inhibits fluorite in this system [10,27]. Figure 4c shows the SS dose as a function of minerals floatability at pH 10. When the dose of SS is low, the floatability of bastnaesite decreases slightly, and the floatability of fluorite decreases rapidly. With increasing SS, the recovery of bastnaesite and fluorite obviously decrease. When the dose of SS is 40 mg/L, the floatability of bastnaesite and fluorite varies greatly, and selective inhibition is the most obvious.

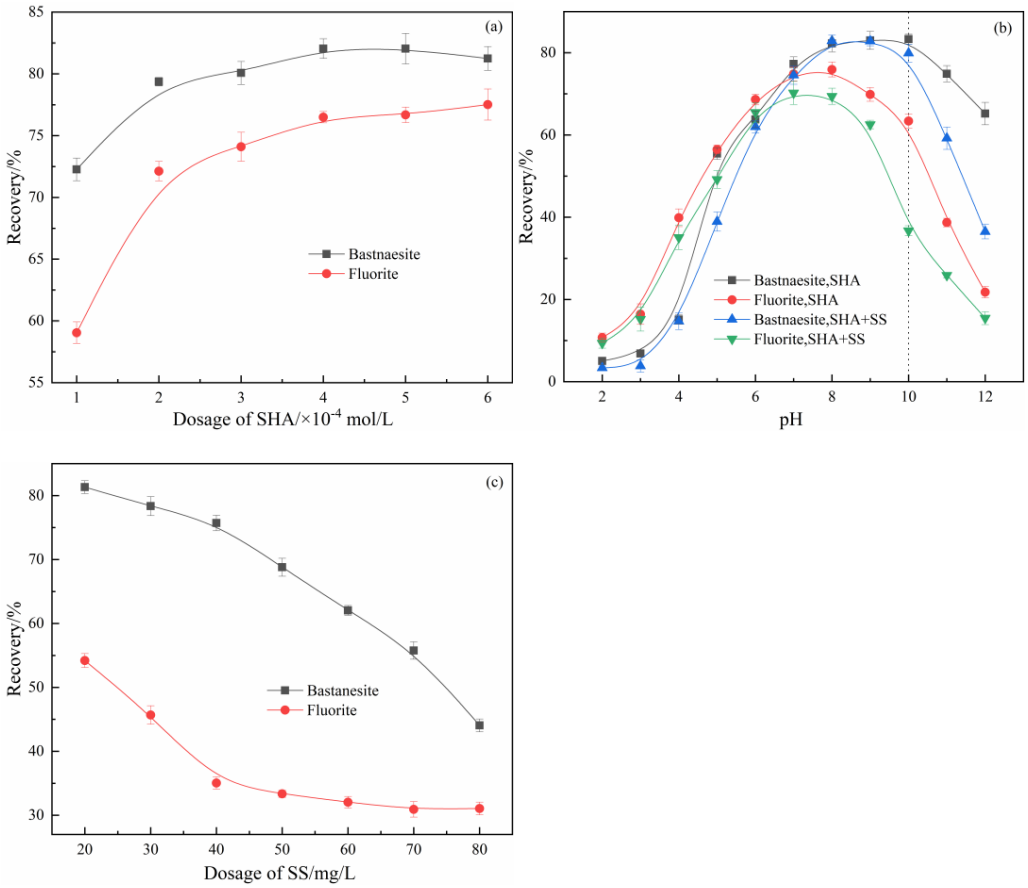

Figure 4. Recoveries of bastnaesite and fluorite as a function of dosages of SHA (**a**: Terpineol 20 mg/L; pH 8), pH (**b**: Terpineol 20 mg/L; SHA 4 × 10^{-4} mol/L; SS 40 mg/L) and dosages of SS (**c**: Terpineol 20 mg/L; SHA 4 × 10^{-4} mol/L; pH 10), respectively.

3.1.2. Flotation Separation Tests of Mixed Ore

Pure mineral flotation experiments show that the best flotation separation conditions of bastnaesite and fluorite were 4 × 10^{-4} mol/L of SHA, 40 mg/L of SS and 20 mg/L of terpineol, pH 10. In order to further determine the flotation results of a single mineral, the bastnaesite and fluorite were mixed manually, according to the mass ratio of 1:1, and the mixed mineral was used for flotation. Table 3 shows the flotation test results.

Table 3. The results of flotation separation of artificial mixed ore.

Reagents	Product	Yield (%)	Grade (%)	Recovery (%)
			Bastnaesite	Bastnaesite
pH: 10; SHA: 4 × 10^{-4} mol/L; T: 20 mg/L	Concentrate	69.23	57.28	79.34
	Tailing	30.77	33.56	20.66
	Feed	100.00	49.98	100.00
pH: 10; SHA: 4 × 10^{-4} mol/L; SS: 40 mg/L; T:20 mg/L	Concentrate	49.67	82.08	83.21
	Tailing	46.99	17.01	16.79
	Feed	100.00	49.98	100.00

Table 3 shows that bastnaesite recovery is 79.34% in the concentrate without SS, but the grade of bastnaesite is only 61.28%. After adding 40 mg/L SS, the recovery and grade of bastnaesite increased to 83.21% and 82.08%, respectively. These figures indicate that SS can effectively separate bastnaesite and fluorite at pH 10.

3.2. Potentiodynamic Measurements

The change of the Zeta potential on the mineral surface can indirectly represent the adsorption of flotation agents on the mineral surface under different pH conditions [28,29]. Figure 5 shows that the isoelectric points of bastnaesite and fluorite are 7.21 and 9.12, respectively, demonstrating the Zeta potentials of bastnaesite and fluorite before and after interaction with different reagents [28,30]. When SHA was used as the sole treatment, the Zeta potentials of bastnaesite and fluorite were negatively shifted as a result of adsorption between SHA and the mineral. After the zero point, the Zeta potentials of bastnaesite and fluorite were still negatively shifted, indicating chemisorption between SHA and the mineral [26,31].

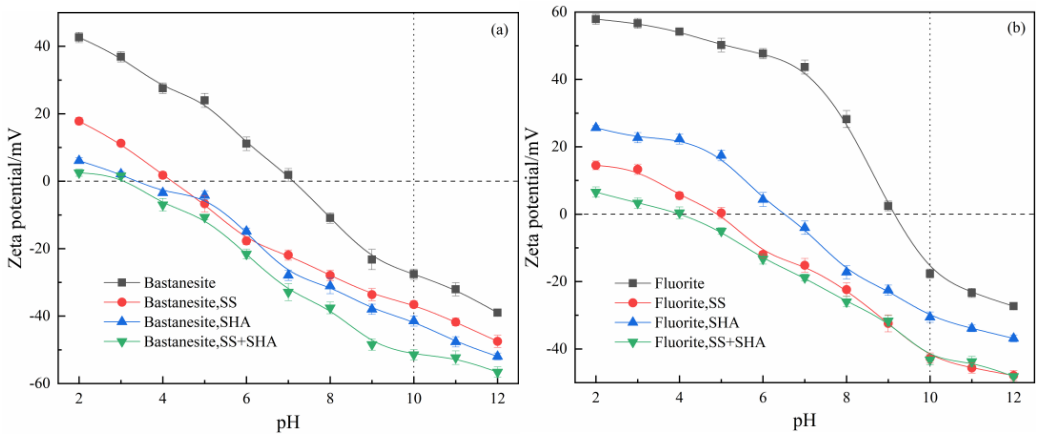

Figure 5. Zeta potentials of the minerals before (**a**) and after (**b**) treatment with reagents (SHA 4×10^{-4} mol/L; SS 20 mg/L).

When SS was added alone, the Zeta potential of bastnaesite shifted slightly in a negative direction, indicating an interaction between the SS components and bastnaesite. The negative shift of the Zeta potential of fluorite over the whole pH range indicates that the interaction between the SS and fluorite is stronger, and there is also chemisorption, in addition to electrostatic adsorption [32]. More precisely, at pH 10, the Zeta potential of the bastnaesite shifts by −6.43 mV (from −29.23 mV to −35.66 mV), and the Zeta potential of the fluorite shifts by −25.48 mV (from −18.91 mV to −44.39 mV).

When adding SS and SHA, the Zeta potential of the bastnaesite still shows a significant negative shift at pH 10 from −29.23 mV to −53.11 mV. These results show that SHA can adsorb on the surface of bastnaesite, even in the presence of SS, and the Zeta potential shift of bastnaesite is more obvious under the action of SHA, which indicates that the adsorption capacity of SS on the surface of bastnaesite is weaker than SHA, which is the reason for the good floatability of bastnaesite at a low SS concentration [33,34]. However, the Zeta potential after both SS and SHA treatment of the fluorite was almost the same as that of the fluorite interacting with SS alone, indicating that adsorption on the SS fluorite surface was stronger than that on SHA. The results show that the presence of SS hinders the further adsorption of SHA on the fluorite surface. Therefore, SS has a stronger inhibitory effect on fluorite than bastnaesite.

3.3. Adsorption Capacity and Solution Chemistry

Figure 6 shows the experimental results of SHA adsorption on the bastnaesite and fluorite surfaces with/without SS. Figure 6a shows that without SS, the maximum adsorption amount of fluorite is at pH 7–8, and the maximum adsorption amount of bastnaesite is at pH 8–10. When adding SS and pH > 9.5, the presence of SS leads to a significant decrease in the adsorption amount of SHA on the fluorite surface. The adsorption experiments shown in Figure 6b investigate the effect of SS dose on SHA adsorption at pH 10. When the dose of SS is low, SHA adsorption on the surface of the bastnaesite is slightly reduced, while SHA adsorption on the surface of the fluorite is greatly reduced. The inhibition of SHA

adsorption on the fluorite surface by SS indicates that SS has a stronger adsorption capacity on fluorite than SHA, which may also explain the results of the single mineral flotation experiments. This phenomenon may be due to the chemical reaction between SS and the fluorite surface, resulting in more stable substances.

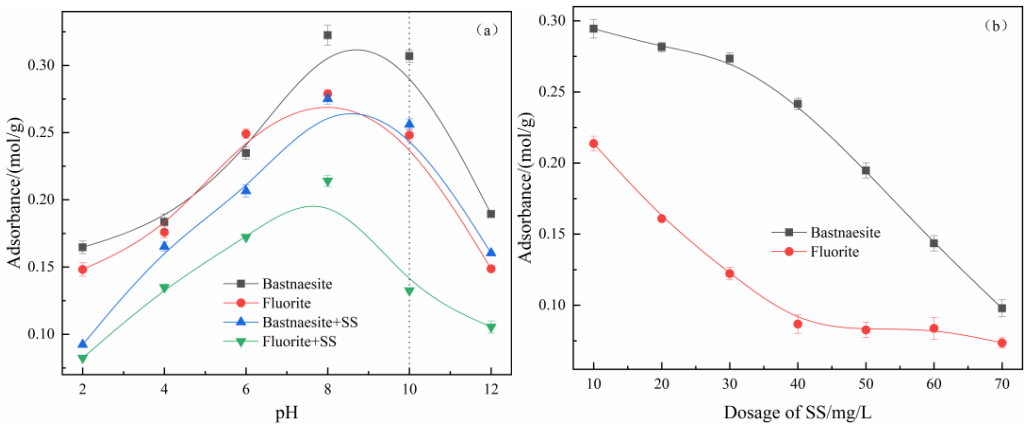

Figure 6. Adsorption of bastnaesite and fluorite as a function of pH (**a**: SHA 4×10^{-4} mol/L; SS 20 mg/L), and dosages of SS (**b**: SHA 4×10^{-4} mol/L; pH 10), respectively.

In the flotation process, the inhibitor in pulp shows various shapes under different pH conditions, and the form of the inhibitor has a certain influence on the flotation performance [29,31,35]. The solution chemistry of SS can be analyzed to obtain the distribution coefficients of each component at different pH values. Figure 7 shows the functional relationship between the hydrolysis components of SS and pH. When the pH < 9.5, the main component of SS in the solution is $Si(OH)_4$; when the pH is 9.5–12.4, the main component of SS in the solution is $SiO(OH)_3^-$ at pH 9.5–12.5; and when pH $\geq$ 12.5, the main component of SS in the solution is $SiO_2(OH)_2^{2-}$ [36,37]. When SS acts, the pH of the slurry is 9.5–12, and the main component in the solution is $SiO(OH)_3^-$. Silicate particles adsorb on the fluorite surface with high solid strength and a large adsorption capacity, which reduces fluorite recovery. In contrast, the adsorption capacity of bastnaesite is small, and the fixation strength is weak. Thus, SS has good selectivity [35,38]. At pH 9.5–12.5, SS has the strongest adsorption capacity on the fluorite surface, which explains why SHA adsorbed on the fluorite surface decreases significantly in this pH range and further verifies the results of the single mineral flotation test.

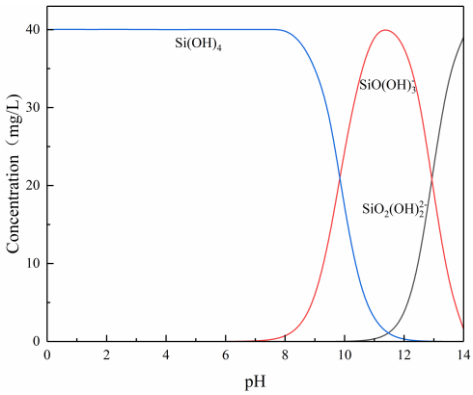

Figure 7. Distribution diagram of silicate ions as a function of pH in 40 mg/L SS.

3.4. Infrared Spectroscopy Analysis

The interference of SS adsorption on bastnaesite and fluorite on SHA was studied by infrared spectrum analysis of SS, SHA and treated bastnaesite and fluorite. The spectra of SHA and SS are shown in Figure 8. Table 4 shows the main bands corresponding to the

relevant chemical bonds. In the FTIR spectra of SHA, 3283 cm^{-1} and 3050 cm^{-1} are the stretching vibrations of -OH with CH_3 on the benzene ring [38,39]; the spectra of 1521 cm^{-1} and 1153 cm^{-1} correspond to the stretching vibrations of benzene rings C=C and C=O, respectively. The spectra at 903 cm^{-1} and 1031 cm^{-1} are the asymmetrical and symmetrical tensile vibrations of -C-N and =N-O, respectively, which are major functional groups of SHA [39]. In the infrared spectrum of SS, the absorption peaks of 3335 cm^{-1} and 1660 cm^{-1} are the -OH stretching vibration and bending vibration absorption peaks of SS, and the absorption peaks of 995 cm^{-1} are the Si-O stretching vibration absorption peaks of SS at 995 cm^{-1} [40].

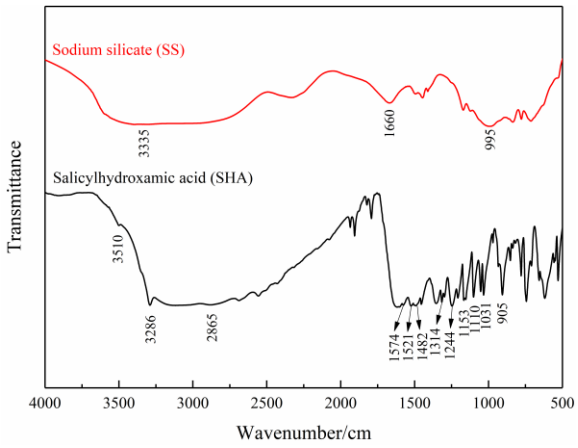

Figure 8. The infrared spectra of SHA and SS.

Table 4. The bands corresponding to the relevant chemical bond in FT-IR spectra of the minerals.

FTIR	Band (cm^{-1})	Chemical Bond
SHA	3286	O-H stretching vibration
	2865	$-CH_3$ stretching vibrations
	1574	C=C stretching vibrations
	1153	C-O stretching vibrations
	1031	=N-O anti-symmetric stretching vibration
	905	N-O symmetric stretching vibration
Bastnaesite	3584	-OH stretching vibration
	1824	C=O and cation coordination
	1445	CO_3^{2-} anti-symmetric stretching vibration
	1087	CO_3^{2-} symmetric stretching vibration
	867	CO_3^{2-} plane bending vibration
	723	CO_3^{2-} in-plane bending vibration
Bastnaesite + SS + SHA	3793	N-H stretching vibrations
	3696	C-H stretching vibrations
	1035	N-O stretching vibrations
	1018	N-O stretching vibrations

Figure 9a shows the infrared spectra of SHA- and SS-treated bastnaesite. The characteristic peak at 3584 cm^{-1} in the pure bastnaesite is due to the -OH stretching vibration from water in the air or on the surface of the sample, which indicates that the ions are hydroxylated at pH 10 and that the planar bending vibration and asymmetric stretching vibration of 2503 cm^{-1} in bastnaesite occur [41]. The peaks at 1824 cm^{-1} and 1763 cm^{-1} are attributed to stretching caused by the coordination between the C=O bond and rare-earth element cations [39]. The bands at 1445 cm^{-1} and 1085 cm^{-1} are attributed to the asymmetric stretching of carbonate. The bands at 867 cm^{-1} and 723 cm^{-1} are the out-of-plane and in-plane bending of carbonate [39,42]. After the ore is treated with SS alone, there is no

SS band, indicating that SS is not obviously adsorbed on the bastnaesite surface. After SS and SHA treatment, the spectrum of bastnaesite shows the characteristic peaks of tensile vibration of C-O and N-H at 3793 cm^{-1}, 3696 cm^{-1}, 3660 cm^{-1} and 3584 cm^{-1}, and the characteristic peaks of out-of-plane bending of =N-O are at 1035 cm^{-1} and 1018 cm^{-1} [39,41,42]. The results show that the presence of SS does not affect the adsorption of SHA on the bastnaesite surface.

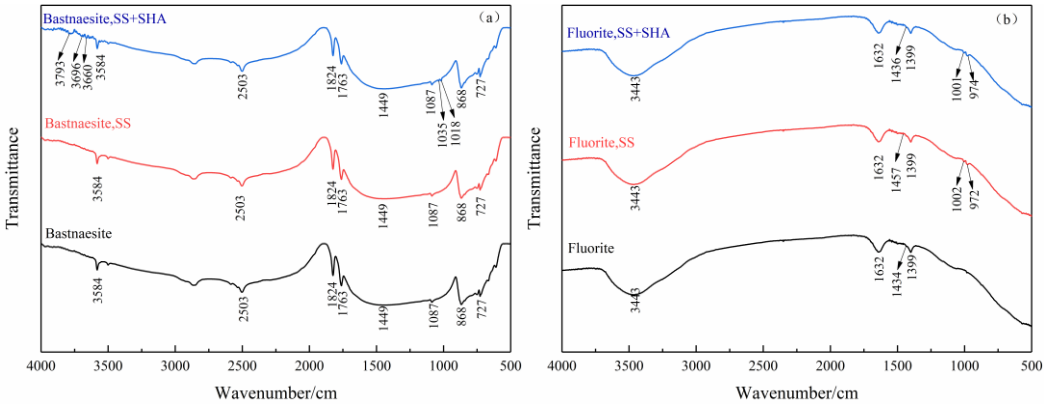

Figure 9. FTIR spectra of pure, SS- and SS+ SHA-treated bastnaesite (**a**) and pure, SS- and SS+ SHA-treated fluorite (**b**).

Figure 9b shows the infrared spectrum of fluorite before and after SS and SHA treatment. For fluorite, the broad peaks near 3443 cm^{-1} and 1632 cm^{-1} are attributed to adsorbed water molecules, and the characteristic peaks at 1434 cm^{-1} and 1399 cm^{-1} are attributed to fluorite [43,44]. After SS treatment, there are new characteristic peaks at 1002 cm^{-1} and 974 cm^{-1} on the fluorite surface, which may be caused by the tensile vibration of Si-O, indicating that there are $SiO(OH)_3^-$ groups on the fluorite surface [45]. Moreover, the characteristic peak of fluorite at 1434 cm^{-1} moves to 1457 cm^{-1}, indicating that SS is adsorbed on the fluorite surface [45,46]. There are no new characteristic peaks on the fluorite surface treated with SHA and SS, unlike that of the surface treated with SS alone. FTIR analysis showed that the surface of the bastnaesite treated with SS did not affect the further adsorption of SHA. When SS and SHA are both used as treatments, the IR spectra of the fluorite are very similar to those of the SS alone. SS can hinder SHA adsorption behavior on the fluorite surface, which further confirms that SS selectively inhibits the fluorite surface, thereby reducing fluorite floatability.

3.5. XPS Measurement Results

Table 5 shows the change of the relative atomic concentration before and after the interaction of the flotation reagent with bastnaesite and fluorite. After SS treatment, the atomic concentrations of C, Ce, La and F decreased slightly, while the atomic concentrations of O and Si only slightly increase [47,48]. After SS and SHA treatment, the C and N atomic concentrations increase by 7.43% and 2.12%, respectively; the Si atomic concentration increases slightly; the O, Ce and La atomic concentrations decrease by 7.28%, 1.00% and 1.36%, respectively; and the F atomic concentration decreases slightly. When compared with bastnaesite, the relative atomic concentration of the fluorite surface treated with SS changes significantly. The atomic concentrations of F, Ca and C decrease by 3.59%, 1.56% and 0.7%, respectively, and the atomic concentrations of O and Si increase by 3.83% and 2.02%, respectively. Especially, significant changes in the Si content suggest that a lot of SS is adsorbed on the fluorite surface. Consequently, the adsorption behavior of the flotation reagents on the mineral surface was further studied. Figure 10 shows the XPS spectra of minerals treated with/without flotation reagents. Figure 10a shows that after adding SS alone, there is no obvious change in the spectrum of the bastnaesite. After the interaction between SS and SHA, a new N 1s peak appears on the surface of the bastnaesite, and SS

does not affect the adsorption of SHA on the surface of the bastnaesite. Figure 10b shows that after adding SS alone, the spectrum of the fluorite shows a new peak at Si 2p, and there are no new peaks where SS and SHA coexist, indicating that a large amount of SS covers the surface of the fluorite, and the presence of SS hinders the adsorption of SHA on the fluorite.

Table 5. Atomic concentrations of various elements on the surfaces of bastnaesite and fluorite untreated and treated by flotation reagents.

Samples	Atomic Concentration/%							
	C	N	O	Ce	La	Ca	F	Si
Bastnaesite	32.51	-	44.70	4.53	6.65	-	11.61	-
SS treated bastnaesite	31.96	-	45.12	4.49	6.61	-	10.84	0.98
SS + SHA treated bastnaesite	39.94	2.12	37.42	3.53	5.29	-	11.01	0.69
Fluorite	13.57	-	5.16	-	-	27.63	53.64	-
SS treated fluorite	12.87	-	8.99	-	-	26.07	50.05	2.02
SS + SHA treated fluorite	12.93	0.12	8.97	-	-	26.02	49.93	2.03

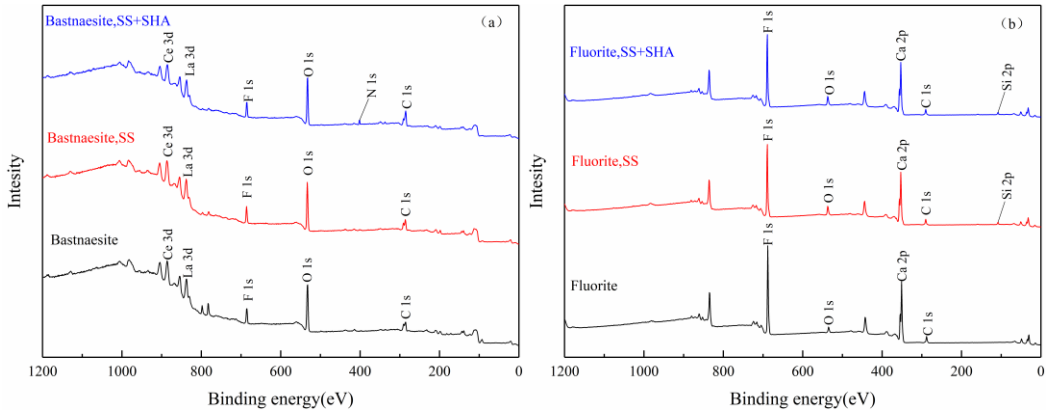

Figure 10. XPS spectra of pure, SS- and SS+ SHA-treated bastnaesite (**a**) and pure, SS- and SS+ SHA-treated fluorite (**b**).

Figure 11a shows the high-definition Ce $3d_{5/2}$ XPS spectra of the pure and flotation reagent-treated bastnaesite samples, and the detailed analysis results of the Ce $3d_{5/2}$ XPS spectra are shown in Table 6. In the pure bastnaesite spectra, the three-dimensional Ce spectrum consists of spin-orbital split $3d_{5/2}$ and $3d_{3/2}$ nuclear pores, and $3d_{5/2}$ is closely linked to the $3d_{3/2}$ spectrum. In general, the binding energy of $3d_{3/2}$ is 18–19 eV higher than that of $3d_{5/2}$, and the intensity ratio between $3d_{5/2}$ and $3d_{3/2}$ is 1.5 [49,50]. For the sake of clarity, only the Ce $3d_{5/2}$ spectrum is analyzed and displayed in this study. The peaks of 888.18 eV and 888.18eV are more likely to be related to Ce (III), which may be due to the complex electron configuration of Ce atoms and the effect of F atoms on the crystal structure of bastnaesite [50,51]. The Ce $3d_{5/2}$ slightly shifted (<0.10) after adding SS alone, all within the instrument error range [52]. When SS and SHA were added together, the Ce $3d_{5/2}$ peak near 531.55 eV decreased by 0.16 ± 0.02 eV. The decrease in binding energy indicates that the SHA is chemically adsorbed on the Ce ions on the surface of the bastnaesite.

Figure 11b shows the high-resolution C 1s XPS spectra of the pure and flotation reagent-treated bastnaesite samples, and the detailed analysis results of the C 1s XPS spectra are shown in Table 7. The results show that the C 1s XPS spectra of pure bastnaesite have two peaks at the binding energies of C-C and CO_3^{2-} of 284.77 eV and 289.31 eV, respectively. The results show that the C 1s XPS spectra of pure bastnaesite can have two component peaks at binding energies of 284.77 eV and 289.31 eV from C-C and CO_3^{2-}, respectively [53,54]. In the C 1s XPS spectra of the bastnaesite treated by SS alone, there is no obvious shift of the C 1s peak, while the peaks at 284.77 eV and 289.31 eV move forward by 0.24 eV and 0.40 eV,

respectively, after SS and SHA treatment. This shift may be due to the superposition of the SHA C=O group with CO_3^{2-} on the surface of the bastnaesite [55].

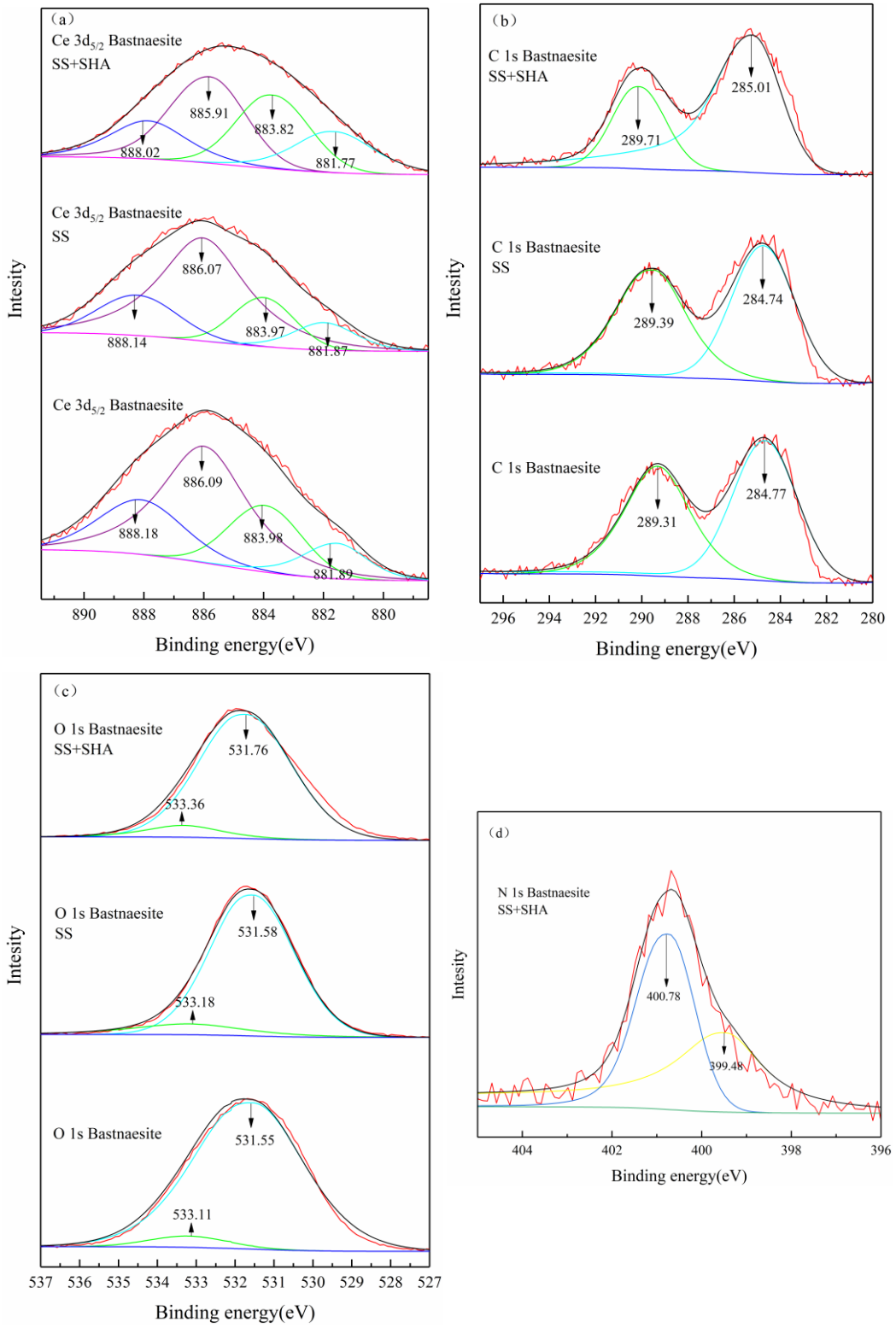

Figure 11. High-resolution XPS spectra of Ce $3d_{5/2}$ (**a**), C 1s (**b**), O 1s (**c**) and N 1s (**d**) of pure, SS- and SS+ SHA-treated bastnaesite particles, respectively.

Table 6. Analysis results of Ce $3d_{5/2}$ XPS spectra of bastnaesite samples untreated and treated by flotation reagent.

Samples	Binding Energy/eV	FWHM/eV	Chemical Shift/eV
Bastnaesite	881.89	2.54	/
	883.98	2.54	/
	886.09	2.54	/
	888.18	2.54	/
Bastnaesite + SS	881.87	2.51	−0.02
	883.97	2.52	−0.01
	886.07	2.51	−0.02
	888.14	2.53	−0.04
Bastnaesite + SS + SHA	881.77	2.63	−0.12
	883.82	2.61	−0.16
	885.91	2.63	−0.18
	888.02	2.63	−0.16

Table 7. Analysis results of C 1s XPS spectra of bastnaesite samples untreated and treated by flotation reagent.

Samples	Binding Energy/eV	FWHM/eV	Chemical Shift/eV
Bastnaesite	284.77	1.81	/
	289.31	1.83	/
Bastnaesite + SS	284.74	1.81	−0.03
	289.39	1.80	0.08
Bastnaesite + SS + SHA	285.01	1.86	0.24
	289.71	1.87	0.40

Figure 11c shows the high-definition O 1s XPS spectra of the pure and flotation reagent-treated bastnaesite samples, and the detailed analysis results of the O 1s XPS spectra are shown in Table 8. The results show that the O 1s region of the bastnaesite can be fitted to two central peaks of binding energy of 531.55 eV and 533.11 eV in the XPS spectra, respectively, from CO_3^{2-} and Ce-OH [55,56]. In the O 1s XPS spectrum of the bastnaesite treated by SS alone, the O 1s XPS peak of CO_3^{2-} moves 0.10 in the positive direction. In the O 1s XPS spectrum of SS- and SHA-treated bastnaesite, the O 1s XPS peak of CO_3^{2-} shifted to the positive direction by 0.24 eV, which is due to the benzene-ring-binding -OH group in SHA [55]. The O 1s XPS peak in the Ce-OH shifts 0.20 eV in the positive direction due to the reaction of the C=O group of the SHA with the surface of the bastnaesite [57].

Table 8. Analysis results of O 1s XPS spectra of bastnaesite samples untreated and treated by flotation reagent.

Samples	Binding Energy/eV	FWHM/eV	Chemical Shift/eV
Bastnaesite	531.55	1.73	/
	533.11	1.63	/
Bastnaesite + SS	531.58	1.48	0.03
	533.18	1.34	0.07
Bastnaesite + SS + SHA	531.76	1.78	0.21
	533.36	1.67	0.25

In addition, Figure 11d shows the high-definition N 1s XPS spectra of the flotation reagent-treated bastnaesite samples, and the detailed analysis results of N 1s XPS spectra are shown in Table 9. It is further confirmed that NHA is adsorbed on the bastnaesite

surface. This adsorption may be attributed to the N atom in the =N-OH forming a new saturated chelate with the surface of the bastnaesite [24,58].

Table 9. Analysis results of N 1s XPS spectra of bastnaesite samples untreated and treated by flotation reagent.

Samples	Binding Energy/eV	FWHM/eV	Chemical Shift/eV
Bastnaesite + SS + SHA	399.48 400.78	1.57 1.47	399.48 400.78

Figure 12a shows the high-definition Ca 2p XPS spectra of the pure and flotation reagent-treated fluorite samples, and the detailed analysis results of the N 1s XPS spectra are shown in Table 10. In the spectra of the pure fluorite samples, the binding energies at 347.74 eV and 351.25 eV are the peaks of Ca $2p_{3/2}$ and Ca $2p_{1/2}$, respectively. In the XPS spectra of the fluorite samples treated by SS alone, the binding energy offsets of the Ca $2p_{3/2}$ and Ca $2p_{1/2}$ peaks are 0.39 eV and 0.27 eV (>0.20 eV), respectively. The obvious shift of the Ca 2p energy spectrum on the fluorite surface indicates that the interaction between the fluorite and the SS is chemical bonding rather than simple physical bonding. This observation shows the chemical surroundings of the fluorite surface has changed. However, the Ca 2p peak of the SS- and SHA-treated fluorite shows no significant change compared with the SS alone [59].

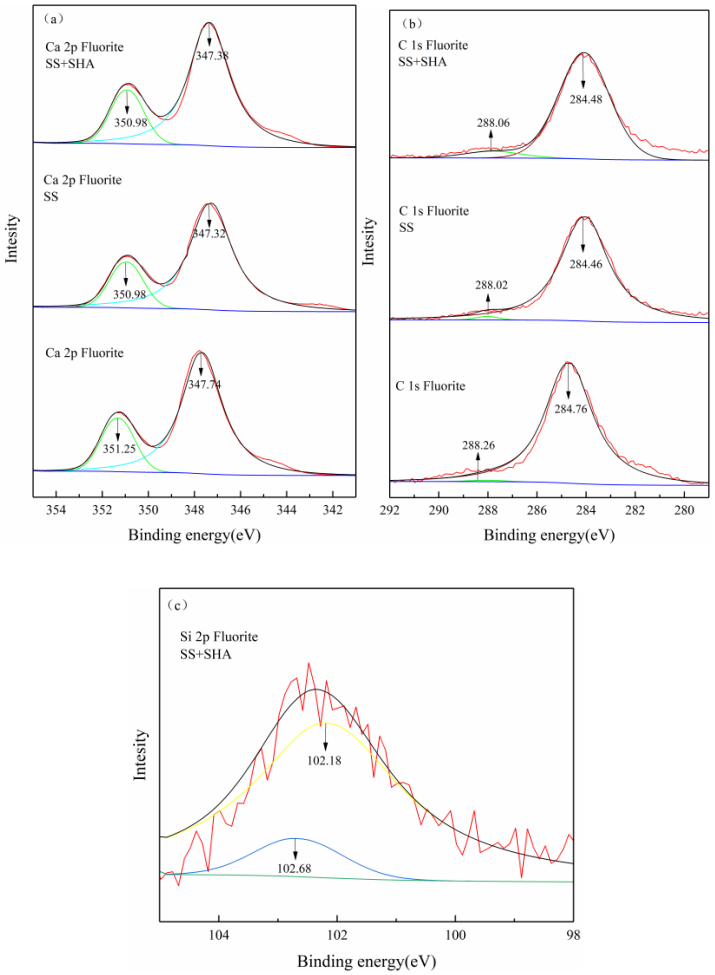

Figure 12. High-resolution XPS spectra of Ca 2p (**a**), C 1s (**b**) and Si 2p (**c**) of pure, SS- and SS+SHA-treated fluorite particles, respectively.

Table 10. Analysis results of Ca 2p XPS spectra of fluorite samples untreated and treated by flotation reagent.

Samples	Binding Energy/eV	FWHM/eV	Chemical Shift/eV
Fluorite	347.74 351.25	2.05 2.05	/ /
Fluorite + SS	347.32 350.98	2.24 2.24	−0.42 −0.27
Fluorite + SS + SHA	347.38 350.98	2.15 2.15	−0.36 −0.27

Figure 12b shows the high-definition C 1s XPS spectra of the pure and flotation reagent-treated fluorite samples, and the detailed analysis results of the C 1s XPS spectra are shown in Table 11. In the spectra of the pure fluorite samples, the C 1s peak is attributed to CO_3^{2-} [24]. In the XPS spectra of the fluorite samples treated with SS alone, the binding energy of the C 1s peak shifts to 0.30 eV and 0.24 eV [24,59]. The fluorite samples treated with SS and SHA did not show the characteristic peaks of the carbonyl groups and the benzene ring of SHA. The binding energy offset of the C 1s peak is less than 0.10 eV, which is within the range of instrument error.

Figure 12c shows the high-definition Si 2p XPS spectra of the flotation reagent-treated fluorite samples, and the detailed analysis results of the Si 2p XPS spectra are shown in Table 12. At 102.16 ev and 102.69 ev, the Si 2p peak of the fluorite was fitted by double peaks [35,37,45]. Because the binding energy of the Si-C bond does not exceed 102 eV near 100.5 eV, it is possible that the SS interacts with the Ca^{2+} on the surface of the fluorite to form a new chemical bond [37,45,60], indicating that the SS is adsorbed on the fluorite. The results show that the SS has chemisorption on the fluorite surface, and the adsorption capacity is higher than that of the bastnaesite.

Table 11. Analysis results of C 1s XPS spectra of fluorite samples untreated and treated by flotation reagent.

Samples	Binding Energy/eV	FWHM/eV	Chemical Shift/eV
Fluorite	284.76 288.26	2.21 2.21	/ /
Fluorite + SS	284.46 288.02	2.44 2.44	−0.30 −0.24
Fluorite + SS + SHA	284.48 288.06	3.88 3.88	−0.28 −0.20

Table 12. Analysis results of Si 2p XPS spectra of fluorite samples untreated and treated by flotation reagent.

Samples	Binding Energy/eV	FWHM/eV	Chemical Shift/eV
Fluorite + SS + SHA	102.18 102.68	2.01 1.51	102.18 102.68

3.6. Discussion

By previous detection and analysis, we found that SS chelates strongly with Ca^{2+} on the fluorite surface at pH 10, but has little interaction with Ce^{3+} on the bastnaesite surface. The chelation reaction between SS and calcium ions was formulated as follows. In each cell, $SiO(OH)_3^-$ provides a pair of oxygen atoms with Ca^{2+} to form a chelation.

$$Ca^{2+}{}_{<surf.>} + SiO(OH)_3^- \longrightarrow Ca^{2+} - OSi(OH)_{3<surf.>} \quad (2)$$

$$Ca^{2+} - F_{<surf.>} + NaSiO(OH)_3^- \longrightarrow Ca^{2+} - OSi(OH)_{3<surf.>} \quad (3)$$

Under the alkaline condition (pH > 10), the $SiO(OH)_3^-$ concentration in the solution is higher, SS can be firmly adsorbed on the fluorite surface, and then the fluorite flotation has a fine inhibition effect [19,37,38,45]. These results indicate that SS is more easily adsorbed on the fluorite surface under specific pH conditions, and a large amount of SS on the fluorite surface interferes with further adsorption of SHA on the fluorite surface [37]. Conversely, only a little SS was adsorbed on the surface of bastnasite, which did not significantly affect the further adsorption of SHA on the surface of the bastnasite. The adsorption model of flotation reagents on the surface of two minerals is shown in Figure 13.

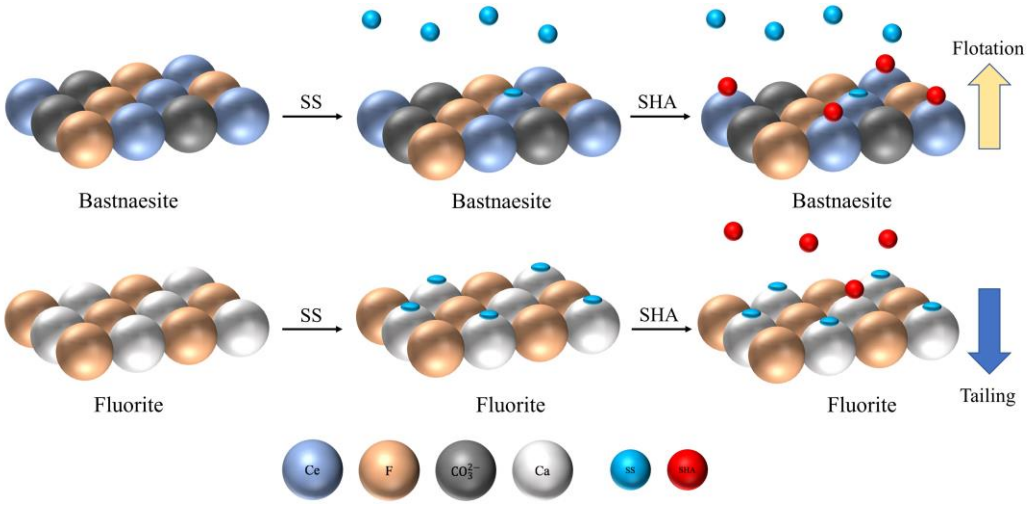

Figure 13. Reaction of flotation reagents with the bastnaesite and fluorite surfaces.

4. Conclusions

The efficient and economical inhibitor SS has been shown to promote the separation of bastnaesite from fluorite. The following is a summary of the study:

(1) The results of micro-flotation show that SS has strong selective inhibition of fluorite in a SHA flotation system. At a pH of 10, SS dosage 40 mg/L and SHA dosage 4×10^{-4} mol/L, the flotation separation effect of bastnaesite and fluorite can be improved, and accurate recovery of bastnaesite is realized.

(2) The potentiodynamic potential and adsorption capacity showed that at pH = 10, the presence of SS did not affect the further adsorption of SHA on the surface of bastnaesite, but the adsorption of SHA on the surface of fluorite was greatly hindered, which may be caused by the selective adsorption of $SiO(OH)_3^-$ ions on the surface of fluorite. Under different pH conditions, the adsorption behavior of hydrolysates of SS on the surface of the two minerals with different strengths leads to the difference in the final floatability of the two minerals, which is the key to achieving flotation separation.

(3) FTIR and XPS analysis showed that SS has a strong binding force with Ca^{2+} on the fluorite surface, while Ce^{3+} had a weak reaction with the bastnaesite surface. This also explains that the selective inhibition of SS on fluorite in flotation separation is determined by the different intensity of action of $SiO(OH)_3^-$ ions on the active sites on the surface of the two minerals. This study has theoretically verified the reason why SS can selectively inhibit bastnaesite and fluorite in flotation separation, and provides guidance for the design and development of flotation separation processes in the future.

Author Contributions: M.W.: Data curation, Investigation, Visualization, Writing original draft. W.X.: Writing—review & editing. J.X.: Methodology, Investigation. Y.G. and J.D.: Software, Validation. D.C.: Funding acquisition, Supervision. A.O. and M.L.: Visualization. L.Z.: Funding acquisition, Supervision. M.L. All authors have read and agreed to the published version of the manuscript.

Funding: The authors gratefully acknowledge the financial support of the Youth Talent Project of the China Ministry of Natural Resources, grant number B1901, 12110600000018003914.

Acknowledgments: The authors gratefully acknowledge the financial support of the Youth Talent Project of the China Ministry of Natural Resources, grant number B1901, 12110600000018003914.

Conflicts of Interest: The authors declare that they have no known competing financial interests or personal relationships that could have appeared to influence the work reported in this paper.

References

1. Zhang, W.; Rezaee, M.; Bhagavatula, A.; Li, Y.; Groppo, J.; Honaker, R. A review of the occurrence and promising recovery methods of rare earth elements from coal and coal by-products. *Int. J. Coal Prep. Util.* **2015**, *35*, 295–330. [CrossRef]
2. Filippov, L.O.; Dehaine, Q.; Filippova, I.V. Rare earths (La, Ce, Nd) and rare metals (Sn, Nb, W) as by-products of kaolin production—Part 3: Processing of fines using gravity and flotation. *Miner. Eng.* **2016**, *95*, 96–106. [CrossRef]
3. Yu, B.; Aghamirian, M. REO mineral separation from silicates and carbonate gangue minerals. *Can. Metall. Q.* **2015**, *54*, 377–387. [CrossRef]
4. Yu, B.; Hu, Z.; Zhou, F.; Feng, J.; Chi, R. Lanthanum (III) and Yttrium (III) Adsorption on Montmorillonite: The Role of Aluminum Ion in Solution and Minerals. *Miner. Process. Extr. Metall. Rev.* **2020**, *41*, 107–116. [CrossRef]
5. Archambo, M.S.; Kawatra, S.K. Extraction of Rare Earths from Red Mud Iron Nugget Slags with Oxalic Acid Precipitation. *Miner. Process. Extr. Metall. Rev.* **2022**, *43*, 656–663. [CrossRef]
6. Talan, D.; Huang, Q.; Liang, L.; Song, X. Conceptual Process Development for the Separation of Thorium, Uranium, and Rare Earths from Coarse Coal Refuse. *Miner. Process. Extr. Metall. Rev.* **2022**, *149*, 1–16. [CrossRef]
7. Cao, S.; Cao, Y.; Ma, Z.; Liao, Y. Metal ion release in bastnaesite flotation system and implications for flotation. *Minerals* **2018**, *8*, 203. [CrossRef]
8. Xiao, J.; Zou, K.; Zhong, N.; Gao, D. Selective separation of iron and scandium from Bayer Sc-bearing red mud. *J. Rare Earths* 2022, *in press*. [CrossRef]
9. Dutta, T.; Kim, K.H.; Uchimiya, M.; Kwon, E.E.; Jeon, B.H.; Deep, A.; Yun, S.-T. Global demand for rare earth resources and strategies for green mining. *Environ. Res.* **2016**, *150*, 182–190. [CrossRef]
10. Jordens, A.; Cheng, Y.P.; Waters, K.E. A review of the beneficiation of rare earth element bearing minerals. *Miner. Eng.* **2013**, *41*, 97–114. [CrossRef]
11. Nduwa-Mushidi, J.; Anderson, C.G. Surface Chemistry and Flotation Behaviors of Monazite–Apatite–Ilmenite–Quartz–Rutile–Zircon with Octanohydroxamic Acid. *J. Sustain. Metall.* **2017**, *3*, 62–72. [CrossRef]
12. Karshigina, Z.; Abisheva, Z.; Bochevskaya, Y.; Akcil, A.; Sargelova, E.; Sukurov, B.; Silachyov, I. Recovery of rare earth metals (REMs) from primary raw material: Sulphatization-leaching-precipitation-extraction. *Miner. Process. Extr. Metall. Rev.* **2018**, *39*, 319–338. [CrossRef]
13. Jordens, A.; Marion, C.; Kuzmina, O.; Waters, K.E. Surface chemistry considerations in the flotation of bastnäsite. *Miner. Eng.* **2014**, *66*, 119–129. [CrossRef]
14. Kupka, N.; Rudolph, M. Froth flotation of scheelite—A review. *Int. J. Min. Sci. Technol.* **2018**, *28*, 373–384. [CrossRef]
15. Fuerstenau, D. The Adsorption of Hydroxamate on Semi-Soluble Minerals. Part I: Adsorption on Barite, Calcite and Bastnaesite. *Colloids Surf.* **1893**, *8*, 103–119.
16. Wang, Z.; Wu, H.; Yang, J.; Tang, Z.; Luo, L.; Shu, K.; Xu, Y.; Xu, L. Selective flotation separation of bastnaesite from calcite using xanthan gum as a depressant. *Appl. Surf. Sci.* **2020**, *512*, 145714. [CrossRef]
17. Xiong, W.; Wang, M.; Xiao, J.; Chen, D. Selective Adsorption of 2-Hydroxy-3-Naphthalene Hydroxamic Acid on the Surface of Bastnaesite and Calcite. *Minerals* **2022**, *12*, 1341. [CrossRef]
18. Yang, Z.; Bian, X.; Wu, W. Flotation performance and adsorption mechanism of styrene phosphonic acid as a collector to synthetic $(Ce,La)_2O_3$. *J. Rare Earths* **2017**, *35*, 621–628. [CrossRef]
19. Marinakis, K.I.; Shergold, H.L. Influence of Sodium Silicate Addition on The Adsorption of Oleic Acid by Fluorite, Calcite and Barite. *Int. J. Miner. Process.* **1985**, *14*, 177–193. [CrossRef]
20. Archambo, M.; Kawatra, S.K. Red Mud: Fundamentals and New Avenues for Utilization. *Miner. Process. Extr. Metall. Rev.* **2021**, *42*, 427–450. [CrossRef]
21. Xiao, J.; Zou, K.; Gao, D.; Zhong, N.; Xiong, W.; Li, C.; Huang, W.; Liang, G. Effective Extraction of Titanium and Iron from Coarse Anatase Concentrate. *JOM* **2022**, *74*, 3833–3842. [CrossRef]
22. Li, W.; Shi, D.; Han, Y. A selective flotation of fluorite from dolomite using caustic cassava starch and its adsorption mechanism: An experimental and DFT Study. *Colloids Surf. A Physicochem. Eng. Asp.* **2022**, *633*, 127876. [CrossRef]

23. Foucaud, Y.; Badawi, M.; Filippov, L.O.; Barres, O.; Filippova, I.V.; Lebègue, S. Synergistic adsorptions of Na_2CO_3 and Na_2SiO_3 on calcium minerals revealed by spectroscopic and: Ab initio molecular dynamics studies. *Chem. Sci.* **2019**, *10*, 9928–9940. [CrossRef] [PubMed]
24. Guo, Z.; Khoso, S.A.; Wang, J.; Zhang, C.; Gao, Z.; Sun, W.; Tian, M.; Liu, Y. Interaction mechanism of 2-hydroxy-3-naphthyl hydroxamic acid and 1-hydroxy-2-naphthyl hydroxamic acid in the flotation separation of bastnaesite/fluorite: Experiments and first-principles calculations. *Sep. Purif. Technol.* **2022**, *285*, 120307. [CrossRef]
25. Qin, W.; Hu, J.; Zhu, H.; Jiao, F.; Pan, Z.; Jia, W.; Han, J.; Chen, C. Selective inhibition mechanism of PBTCA on flotation separation of magnesite from calcite. *Colloids Surf. A Physicochem. Eng. Asp.* **2021**, *630*, 127597. [CrossRef]
26. Yu, X.; Zhang, R.; Zeng, Y.; Cheng, C.; Huang, Z.; Wang, J.; He, G.; Wang, H. The effect and mechanism of cinnamic hydroxamic acid as a collector in flotation separation of malachite and calcite. *Miner. Eng.* **2021**, *164*, 106847. [CrossRef]
27. Wanhala, A.K.; Doughty, B.; Bryantsev, V.S.; Wu, L.; Mahurin, S.M.; Jansone-Popova, S.; Cheshire, M.C.; Navrotsky, A.; Stack, A. Adsorption mechanism of alkyl hydroxamic acid onto bastnäsite: Fundamental steps toward rational collector design for rare earth elements. *J. Colloid Interface Sci.* **2019**, *553*, 210–219. [CrossRef]
28. Gao, Z.; Bai, D.; Sun, W.; Cao, X.; Hu, Y. Selective flotation of scheelite from calcite and fluorite using a collector mixture. *Miner. Eng.* **2015**, *72*, 23–26. [CrossRef]
29. Devi, N.; Sukla, L.B. Studies on Liquid-Liquid Extraction of Yttrium and Separation from Other Rare Earth Elements Using Bifunctional Ionic Liquids. *Miner. Process. Extr. Metall. Rev.* **2019**, *40*, 46–55. [CrossRef]
30. Owens, C.L.; Nash, G.R.; Hadler, K.; Fitzpatrick, R.S.; Anderson, C.G.; Wall, F. Zeta potentials of the rare earth element fluorcarbonate minerals focusing on bastnäsite and parisite. *Adv. Colloid Interface Sci.* **2018**, *256*, 152–162. [CrossRef]
31. Wang, Z.; Wu, H.; Xu, Y.; Shu, K.; Fang, S.; Xu, L. The effect of dissolved calcite species on the flotation of bastnaesite using sodium oleate. *Miner. Eng.* **2020**, *145*, 106095. [CrossRef]
32. Meng, Q.; Feng, Q.; Shi, Q.; Ou, L. Studies on interaction mechanism of fine wolframite with octyl hydroxamic acid. *Miner. Eng.* **2015**, *79*, 133–138.
33. Jiang, W.; Gao, Z.; Khoso, S.A.; Gao, J.; Sun, W.; Pu, W.; Hu, Y. Selective adsorption of benzhydroxamic acid on fluorite rendering selective separation of fluorite/calcite. *Appl. Surf. Sci.* **2018**, *435*, 752–758. [CrossRef]
34. Wang, W.; Wang, H.; Wu, Q.; Zheng, Y.; Cui, Y.; Yan, W.; Deng, J.; Peng, T. Comparative study on adsorption and depressant effects of carboxymethyl cellulose and sodium silicate in flotation. *J. Mol. Liq.* **2018**, *268*, 140–148. [CrossRef]
35. Jin, S.; Ou, L.; Ma, X.; Zhou, H.; Zhang, Z. Activation mechanisms of sodium silicate-inhibited fluorite in flotation under neutral and slightly alkaline conditions. *Miner. Eng.* **2021**, *161*, 106738. [CrossRef]
36. Foucaud, Y.; Filippova, I.V.; Filippov, L.O. Investigation of the depressants involved in the selective flotation of scheelite from apatite, fluorite, and calcium silicates: Focus on the sodium silicate/sodium carbonate system. *Powder Technol.* **2019**, *352*, 501–512. [CrossRef]
37. Zhang, S.; Kuang, J.; Yu, M.; Yuan, W.; Huang, Z. Effect of ultrasonication of sodium silicate on selective adsorption of scheelite and fluorite surfaces. *Colloids Surf. A Physicochem. Eng. Asp.* **2022**, *642*, 128633. [CrossRef]
38. Natarajan, R.; Nirdosh, I. Application of topochemical, topostructural, physicochemical and geometrical parameters to model the flotation efficiencies of N-arylhydroxamic acids. *Int. J. Miner. Process.* **2003**, *71*, 113–129. [CrossRef]
39. Xiong, W.; Deng, J.; Zhao, K.; Wang, W.; Wang, Y.; Wei, D. Bastnaesite, barite, and calcite flotation behaviors with salicylhydroxamic acid as the collector. *Minerals* **2020**, *10*, 282. [CrossRef]
40. Feng, B.; Luo, X.P. The solution chemistry of carbonate and implications for pyrite flotation. *Miner. Eng.* **2013**, *53*, 181–183. [CrossRef]
41. Xiao, J.; Di, N.; Liu, G.; Zhong, H. The interaction of N-butoxypropyl-N′-ethoxycarbonylthiourea with sulfide minerals: Scanning electrochemical microscopy, diffuse reflectance infrared Fourier transform spectroscopy, and thermodynamics. *Colloids Surf. A Phys. Eng. Asp.* **2014**, *456*, 203–210. [CrossRef]
42. Xu, Y.; Xu, L.; Wu, H.; Wang, Z.; Shu, K.; Fang, S.; Zhang, Z. Flotation and co–adsorption of mixed collectors octanohydroxamic acid/sodium oleate on bastnaesite. *J. Alloys Compd.* **2020**, *819*, 152948. [CrossRef]
43. Singh, R.K. FTIR Spectroscpy of Natural Fluorite from Ambadongar, Gujarat. *J. Geol. Soc. India* **2013**, *81*, 215–218. [CrossRef]
44. Dong, L.; Jiao, F.; Qin, W.; Wei, Q. New insights into the depressive mechanism of citric acid in the selective flotation of scheelite from fluorite. *Miner. Eng.* **2021**, *171*, 107117. [CrossRef]
45. Zhang, C.; Hu, Y.; Sun, W.; Zhai, J.; Yin, Z.; Guan, Q. Effect of phytic acid on the surface properties of scheelite and fluorite for their selective flotation. *Colloids Surf. A Phys. Eng. Asp.* **2019**, *573*, 80–87. [CrossRef]
46. Foucaud, Y.; Lainé, J.; Filippov, L.; Barrès, O.; Kim, J.; Filippova, I.; Pastore, M.; Lebègue, S.; Badawi, M. Adsorption mechanisms of fatty acids on fluorite unraveled by infrared spectroscopy and first-principles calculations. *J. Colloid Interface Sci.* **2020**, *583*, 692–703. [CrossRef] [PubMed]
47. Dong, L.; Jiao, F.; Qin, W.; Zhu, H.; Jia, W. Selective depressive effect of sodium fluorosilicate on calcite during scheelite flotation. *Miner. Eng.* **2019**, *131*, 262–271. [CrossRef]
48. Nambaje, C.; Mweene, L.; Subramanian, S.; Sajeev, K.; Santosh, M. Xanthan gum based investigations into the surface chemistry of cassiterite and beneficiation of cassiterite tailings. *Miner. Process. Extr. Metall. Rev.* **2022**, *43*, 150–164. [CrossRef]
49. Qi, J.; Liu, G.; Dong, Y. Probing the hydrophobic mechanism of N-[(3-hydroxyamino)-propoxy]-N-octyl dithiocarbamate toward bastnaesite flotation by in situ AFM, FTIR and XPS. *J. Colloid Interface Sci.* **2020**, *572*, 179–189. [CrossRef]

50. Meng, D.; Wu, X.; Han, Y.; Meng, X. Polytypism and microstructures of the mixed-layer member B_2S, $CaCe_3(CO_3)_4F_3$ in the bastnaesite-(Ce)ˆsynchysite-(Ce) series. *Earth Planet. Sci. Lett.* **2002**, *203*, 817–828. [CrossRef]
51. Qi, J.; Fan, H.; Liu, G. β-Amino-hydroxamate surfactants: Preparation, and adsorption mechanism in bastnaesite flotation. *Sep. Purif. Technol.* **2020**, *240*, 116634. [CrossRef]
52. Vickerman, J.; Gilmore, I.S. *Surface Analysis the Principal Techniques*, 2nd ed.; John Wiley & Sons: Hoboken, NJ, USA, 2011.
53. Espiritu, E.R.L.; da Silva, G.R.; Azizi, D.; Larachi, F.; Waters, K.E. The effect of dissolved mineral species on bastnäsite, monazite and dolomite flotation using benzohydroxamate collector. *Colloids Surf. A Phys. Eng. Asp.* **2018**, *539*, 319–334. [CrossRef]
54. Li, M.; Gao, K.; Zhang, D.; Duan, H.; Ma, L.; Huang, L. The influence of temperature on rare earth flotation with naphthyl hydroxamic acid. *J. Rare Earths* **2018**, *36*, 99–107. [CrossRef]
55. Światowska, J.; Lair, V.; Pereira-Nabais, C.; Cote, G.; Marcus, P.; Chagnes, A. XPS, XRD and SEM characterization of a thin ceria layer deposited onto graphite electrode for application in lithium-ion batteries. *Appl. Surf. Sci.* **2011**, *257*, 9110–9119. [CrossRef]
56. Dauscher, A.; Hilaire, L.; le Normand, F.; Müller, W.; Maire, G.; Vasquez, A. Characterization by XPS and XAS of supported Pt/TiO_2—CeO_2 catalysts. *Surf. Interface Anal.* **1990**, *16*, 341–346. [CrossRef]
57. Mullins, D.R. The surface chemistry of cerium oxide. *Surf. Sci. Rep.* **2015**, *70*, 42–85. [CrossRef]
58. Liu, S.; Liu, G.; Zhong, H.; Yang, X. The role of HABTC's hydroxamate and dithiocarbamate groups in chalcopyrite flotation. *J. Ind. Eng. Chem.* **2017**, *52*, 359–368. [CrossRef]
59. Zhang, Z.; Cao, Y.; Sun, L.; Ma, Z.; Liao, Y. Interaction forces between scheelite and fluorite in calcium solution measured by atomic force microscopy. *Appl. Surf. Sci.* **2019**, *486*, 323–336. [CrossRef]
60. Cao, Z.; Cheng, Z.; Wang, J.; Cao, Y. Synergistic depression mechanism of Ca^{2+} ions and sodium silicate on bastnaesite flotation. *J. Rare Earths* **2022**, *40*, 988–995. [CrossRef]

Disclaimer/Publisher's Note: The statements, opinions and data contained in all publications are solely those of the individual author(s) and contributor(s) and not of MDPI and/or the editor(s). MDPI and/or the editor(s) disclaim responsibility for any injury to people or property resulting from any ideas, methods, instructions or products referred to in the content.